Synthesis, structure, and characterizations of a new antiferromagnetic manganese(II) dichloro-bridged 1-D polymer decorated by 5-amino-1-H-tetrazole

Elena A. Buvaylo, Vladimir N. Kokozay, Olga Yu. Vassilyeva, Brian W. Skelton, Mikhail M. Degtyarik, Maria Korabik & Julia Jezierska

View supplementary material

Submit your article to this journal

View related articles

Accepted author version posted online: 18 Feb 2015.
Published online: 12 Mar 2015.

Article views: 46

View Crossmark data

Taylor & Francis
Taylor & Francis Group

Synthesis, structure, and characterizations of a new antiferromagnetic manganese(II) dichloro-bridged 1-D polymer decorated by 5-amino-1-H-tetrazole

ELENA A. BUVAYLO†, VLADIMIR N. KOKOZAY†, OLGA YU. VASSILYEVA*†,
BRIAN W. SKELTON‡, MIKHAIL M. DEGTYARIK§, MARIA KORABIK¶ and
JULIA JEZIERSKA¶

†Department of Chemistry, Taras Shevchenko National University of Kyiv, Kyiv, Ukraine
‡Centre for Microscopy, Characterisation and Analysis, University of Western Australia, Crawley, Australia
§Research Institute for Physical Chemical Problems of Belarusian State University, Minsk, Belarus
¶Faculty of Chemistry, University of Wroclaw, Wroclaw, Poland
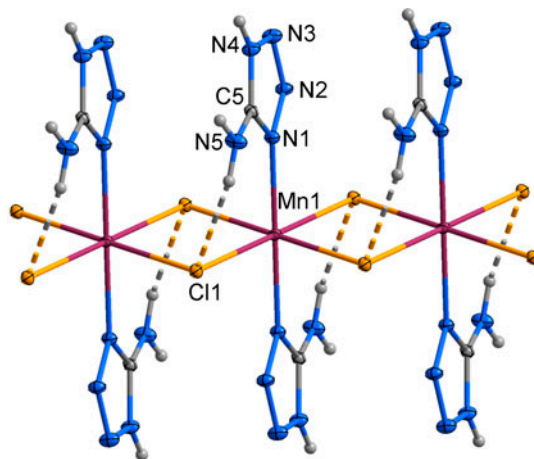
$[Mn(5-ATZ)_2Cl_2]_n$ (**1**) (5-ATZ – 5-amino-1-H-tetrazole) was synthesized from the reaction of 5-ATZ and manganese(II) chloride and isolated by solution evaporation at room temperature. **1** was characterized by elemental analysis, X-ray crystallography, infrared, and EPR spectroscopy as well as magnetic measurements. In the crystal structure, $[Mn(5-ATZ)_2Cl_2]$ units are linked by double μ_2-bridging chlorides to form 1-D chains parallel to the *a*-axis. The Mn sphere approximates to octahedral with the metal coordinated by four chlorides in the equatorial plane and two 5-ATZ molecules, bound through their ring nitrogens, in axial positions. The intramolecular N–H···Cl hydrogen bond between the 5-ATZ amino group and the adjacent coordinated Cl^- stabilizes the chain. N–H···N hydrogen bonds between adjacent chains form a 3-D supramolecular framework. No hyperfine coupling to the Mn nuclei ($I = 5/2$) is observed in the powdered EPR spectrum of **1** at

---

*Corresponding author. Email: vassilyeva@univ.kiev.ua

77 K. The frozen solution EPR spectrum provides evidence of the mononuclearity of **1** in methanol. The magnetic properties have been analyzed using the Hamiltonian $H = -J\sum S_i \cdot S_{i+1}$ with $J = -1.38$ (3) cm^{-1} and $g = 2.00(1)$. A small value of the exchange parameter is typical for 1-D six-coordinate bis(μ_2-chloro) Mn(II) polymers.

1. Introduction

Hybrid inorganic–organic framework compounds are crystalline systems that contain both inorganic and organic moieties as integral parts of a network with infinite bonding connectivity in at least 1-D [1]. Most of the known hybrid frameworks may be divided into two categories according to the connectivity of the inorganic and organic components inside the crystalline hybrid material [2]. The coordination polymers and metal organic frameworks (MOFs) can be defined as extended arrays composed of isolated metal ions or clusters that are connected via organic linkers, L. These are based upon M–L–M connectivity and often contain cavities and channels akin to those found in zeolites. Porous hybrid frameworks are widely studied, particularly in view of their potential applications in catalysis, gas separation, and sensors [3]. In contrast, there are hybrid systems that are dense rather than porous, in which the inorganic structural elements form an infinite array in one, two, or three directions. At present, the vast majority of known materials of the latter type are based upon oxygen bridges (hybrid metal oxides) [1]. Extended inorganic connectivity provides the structural basis for many key physical properties – electronic, magnetic, optical – traditionally found in inorganic materials. The organic component is used to tailor the electronic properties of the inorganic framework by influencing its dimensionality and mediating the electronic coupling between inorganic units. It is believed that there is a great deal of untapped potential in the area of dense hybrids, many of which have excellent stability [4].

A variety of magnetic properties have been found with hybrid inorganic–organic compounds, of particular interest being those with ferromagnetic exchange [5]. Antiferromagnetic materials do not have wide applicability compared with ferromagnetic examples due to their lack of spontaneous magnetization. They are, however, closely related structurally to the spontaneously magnetized ferrimagnets and therefore can provide a simpler system in which to test the theoretical models to explain ferrimagnetism [6]. One area in which antiferromagnets are starting to find wide applicability is in so-called spin valves due to a phenomenon called exchange anisotropy or exchange-bias coupling [7]. Additional applications for antiferromagnetic materials might emerge from current research of solids, which show a phase transition from an antiferromagnetic to a ferromagnetic state, with corresponding changes in structural and magnetic properties [6].

Polymers of divalent metals, which feature bridging halides in addition to the donor ligands, provide a meeting ground between the fields of coordination compounds and classical inorganic and ionic solids [8]. Magnetic properties of the dichloro-bridged d^5 Mn(II) chains with metal ions capped by ligand N/O donors have been described by a number of groups [9] starting with polymeric [A]MnCl$_3$ (A = NMe$_4^+$ and H$_2$NMe$_2^+$), which have been studied as "ideal" 1-D Heisenberg antiferromagnets [10]. A comparison of the structural and magnetic behavior of a series of chloride-bridged octahedral Mn(II) chains demonstrated a linear correlation between the Mn–Cl–Mn bond angle and the magnitude of the intrachain exchange constant [9(g)].

5-Amino-1-H-tetrazole (5-ATZ, CN_5H_3) is a promising multidentate ligand that has demonstrated its coordination versatility affording both acentric mononuclear molecular complexes with unusual magnetic and ferroelectric properties [11], inorganic networks of various dimensionality templated by 5-ATZ anions [12], and novel MOFs constructed with 5-ATZ as an organic linker [13]. In this study, we present the 1-D chain structure and magnetic properties of $[Mn(5\text{-}ATZ)_2Cl_2]_n$ (**1**), that contains monodentate neutral 5-amino-1-H-tetrazole ligand, isolated by solution evaporation at room temperature. **1** shows weak antiferromagnetic properties.

2. Experimental

2.1. *Materials and instrumentation*

Commercially available chemicals were used as received; all experiments were carried out in air. Elemental analysis for Mn was performed by atomic absorption spectroscopy. Elemental analyses for CHN were performed using a Perkin-Elmer 2400 series analyzer. The IR spectrum was recorded on a Perkin-Elmer 1600 FT-IR spectrometer (KBr pellet, 4000–400 cm^{-1}).

Magnetic susceptibility measurements of a powdered sample from 1.8 to 400 K at magnetic field of 5000 G and magnetization measurements at 2 K, between 0 and 50 000 G, were carried out with a SQUID magnetometer (Quantum Design MPMSXL-5). Corrections for the sample holders were applied. Diamagnetic corrections for the molecule were determined from Pascal's constants [14]. X-band (9.8 GHz) EPR spectra were recorded on a Bruker ELEXSYS E500 instrument equipped with an NMR teslameter (ER 036TM) and a frequency counter (E 41 FC) and operating at microwave power of 10 mW, modulation amplitude of 0.5 mT, and 2048 data points per spectrum. The experimental frozen solution spectrum was simulated using the program SPIN ($S > 1/2$) written by Dr. Andrew Ozarowski from NHMFL, University of Florida, with resonance field calculated by full diagonalization of the energy matrix.

2.2. *Synthesis of $[Mn(5\text{-}ATZ)_2Cl_2]_n$ (1)*

To a methanol solution (10 mL) of $MnCl_2 \cdot 4H_2O$ (0.20 g, 1 mM), 5-ATZ (0.34 g, 4 mM) in methanol (10 mL) was added under stirring. The resulting mixture was stirred for 1 h, then filtered and left to evaporate at room temperature. After several days, air-stable, light yellow crystals of **1** were obtained. Yield: 0.22 g, 72% (based on manganese salt). Elemental analysis data: Anal. Calcd (%) for $C_2H_6Cl_2MnN_{10}$ (296.01): C, 8.12; H, 2.04; N, 47.32; Mn, 18.56. Found (%): C, 7.91; H, 2.20; N, 47.50; Mn, 18.82. IR (KBr, ν, cm^{-1}): 3400 s, 3314 s, 3210 m, 3080 s, 3019 s, 1652 s, 1578 s, 1452 s, 1304 s, 1150 m, 1098 m, 1064 s, 1014 m, 788 m, 736 m, 688 m, 520 w, 442 m, 418 m.

2.3. *Single-crystal structure determination*

Crystallographic data for the structure were collected at 100(2) K on an Oxford Diffraction Gemini CCD diffractometer fitted with Mo Kα radiation ($\lambda = 0.71073$ Å). Following analytical absorption corrections and solution by direct methods, the structure was refined against F^2 with full-matrix least squares using SHELXL-97 [15]. Amino group hydrogens were

Table 1. Crystallographic data for **1**.

Formula	$C_2H_6Cl_2MnN_{10}$
Formula weight	296.01
Crystal system	*Monoclinic*
Space group	*P2₁/n*
a (Å)	3.6256(2)
b (Å)	16.1429(11)
c (Å)	8.0673(8)
β (°)	94.420(6)
V (Å³)	470.76(6)
Z	2
Abs. coeff. (mm⁻¹)	1.954
Reflections collected	5806
Independent reflections	1899 (R_{int} = 0.0362)
Data/restraints/parameters	1899/2/80
Goodness-of-fit on F^2	1.081
Final R indices [$I > 2\sigma(I)$]	R_1 = 0.0290, wR_2 = 0.0624
R indices (all data)	R_1 = 0.0396, wR_2 = 0.0665
Largest diff. peak and hole (e Å⁻³)	0.531 and −0.362
CCDC	1006111

refined with restrained geometries. All remaining hydrogens were added at calculated positions and refined by use of a riding model with isotropic displacement parameters based on those of the parent atoms. Anisotropic displacement parameters were employed throughout for the non-hydrogen atoms. The crystal data are summarized in table 1.

3. Results

3.1. *Description of the crystal structure*

Compound **1** crystallizes as light yellow rods in the monoclinic space group *P2₁/n* and is isomorphous with the Cd analog [12]. In the crystal structure, [Mn(5-ATZ)₂Cl₂] units are linked by double μ₂-bridging chlorides to form 1-D chains parallel to the *a*-axis. The
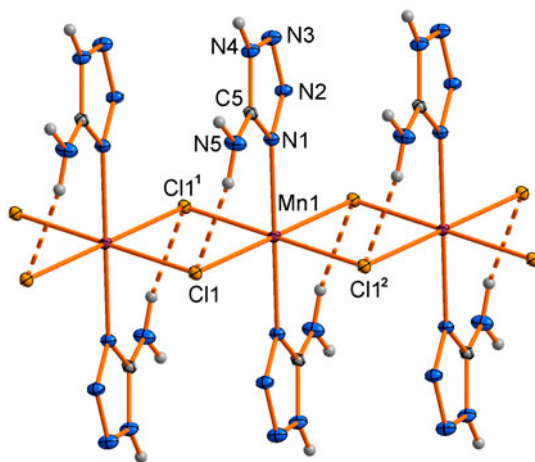

Figure 1. Fragment of the crystal structure of **1** with ellipsoids at 50% probability (H-bonds shown as dashed lines).

Table 2. Selected bond lengths (Å) and angles (°) for **1**.

Mn(1)–N(1)	2.2656(12)	N(1)–Mn(1)–Cl(1)[1]	88.95(3)
Mn(1)–Cl(1)	2.5417(3)	N(1)–Mn(1)–Cl(1)	90.15(3)
Mn(1)–Cl(1)[1]	2.5395(4)	Cl(1)[1]–Mn(1)–Cl(1)	88.955(11)
		Cl(1)[2]–Mn(1)–Cl(1)	91.045(11)
		Mn(1)[3]–Cl(1)–Mn(1)	91.045(11)

Symmetry transformations used: [1]$-x$, $1-y$, $1-z$; [2]$x+1$, y, z; [3]$x-1$, y, z.

geometry of the monomeric units in the coordination polymer is shown in figure 1; selected bond lengths and angles are given in table 2. The manganese is located on a crystallographic inversion center and adopts approximately octahedral coordination. It is coordinated by four chlorides in the equatorial plane (Mn–Cl 2.5417(3), 2.5395(4) Å) and two 5-ATZ molecules, bound through their ring nitrogen atoms (Mn–N 2.2656(12) Å), in axial positions. Bond angles about the metal are close to octahedral with the largest deviation from the ideal value of 90° being 1.045° ($\angle$Cl(1)–Mn–Cl(1)[2]). Similar 1-D chain structural motifs of edge-sharing octahedra with donor ligands in *trans* geometry were observed for pyridine [9(a)], 4-cyanopyridine [9(b)], pyrazole [16(a)], benzotriazole [16(b)], benzo-2,1,3-selenadiazole [16(c)], and acetonitrile [16(d)] Mn(II) chloride complexes of MnL_2Cl_2 composition. In these compounds, average Mn–N, Mn–Cl distances, and acute Cl–M–Cl angles are 2.2–2.3, 2.5–2.6 Å, and 85°–87°, respectively, in accord with our observations. In **1**, the strictly planar Mn_2Cl_2 cores with two almost equal Mn–Cl distances join inversion-related molecules generating essentially flat inorganic $[MnCl_2]_n$ tapes. The intrachain Mn···Mn separation corresponds to the cell length of the *a*-axis (3.6256 Å) and is comparable to those found in other polymeric dichloro-bridged Mn(II) complexes of monodentate donor ligands, 3.700–3.761 Å [9(a), (b), 16].

The 5-amino-1-H-tetrazole in **1** is little affected by coordination to the manganese ions. The similarity of the bond distances and angles with the dimensions of the free molecule [17] indicates there is no electron transfer between the metal and the ligand. The 5-ATZ ligands on opposite sides of the manganese are related by an inversion center and are therefore coplanar. There is an intramolecular hydrogen bond of moderate strength between one hydrogen of the 5-ATZ amino group and the adjacent coordinated Cl atom [N5–H5A···Cl1, 3.2397(14) Å, $\angle = 151.2(18)°$] (figure 1). The other hydrogen of the amino group associates with a non-coordinated ring nitrogen from the 5-ATZ ligand of the neighboring chain to form an intermolecular hydrogen bonding interaction [N5–H5B···N3 {$x-1/2$, $3/2-y$, $z+1/2$}, 3.0432(18) Å, $\angle = 152(2)°$]. The remaining NH group donates its hydrogen to another non-coordinated ring nitrogen from the same 5-ATZ ligand [N4–H4···N2 {$x-1/2$, $3/2-y$, $z+1/2$}, 2.8254(17) Å, $\angle = 157.9°$]. Therefore, a 3-D supramolecular framework is formed (figure 2) with the shortest interchain Mn···Mn distances being 7.251, 8.067 (*c*-axial length), and 8.586 Å.

3.2. *EPR studies*

The EPR spectrum of a powder sample of **1** at 77 K shows a broad resonance at $g = 2$ with width about 460 G (figure S1, see online supplemental material at http://dx.doi.org/10.1080/00958972.2015.1019874) without resolution of the fine structure signals due to resonance transitions between the spin levels split in zero magnetic field. This feature is typical for polymeric Mn(II) complexes [9(d)]. The intermolecular dipolar interaction, ZFS of
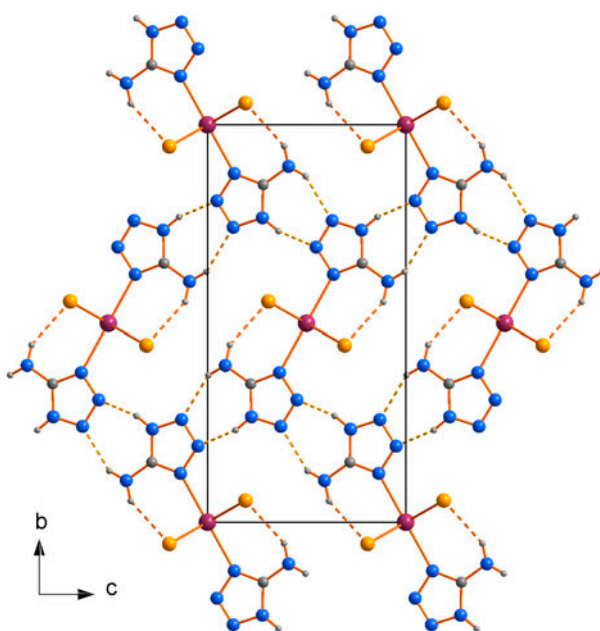
Figure 2.   Fragment of the supramolecular network in **1** (H-bonds shown as dashed lines).
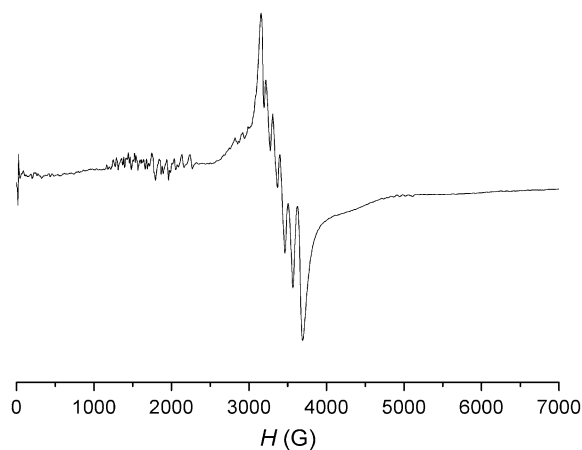

Figure 3.   X-band EPR spectrum of **1** in methanol solution at 77 K.

individual Mn(II) centers, and coupled Mn(II) ions result in broadening of the spectrum and loss of fine structure resolution.

The frozen solution spectrum (77 K) is dominated by the six-line pattern at $g = 2$, with the corresponding hyperfine coupling constant of *ca*. 90 G (figure 3). The spectrum also reveals additional intense signals in the $g = 4.2$ region and very weak multi-line hyperfine splitting at $g \approx 1.4$, both with an average spacing of *ca*. 90 G. The communication between

two Mn(II) centers, often identified by observation of a characteristic 11-line hyperfine pattern with a 45 G average separation [18, 19, and references therein], cannot be established for **1** in the frozen solution. The simulation using the spin Hamiltonian parameters for the individual Mn(II) center, $S = 5/2$, and D about 370–380 G with $g = 2$, produces a pattern that satisfactorily approximates the main features of the experimental spectrum (figure S2, see online supplemental material at http://dx.doi.org/10.1080/00958972.2015. 1019874). The number of the hyperfine splitting lines and the spacing between them clearly evidence the mononuclearity of **1** in methanol [20]. Two sets of hyperfine lines around the $g = 4.2$ transition of the spectrum can be the result of the presence of monomers that slightly differ in the D parameter due to a different mode of solvolysis.

3.3. *Magnetic measurements*

The powder magnetic susceptibility of **1** has been measured between 1.8 and 300 K and the data are presented in figure 4. The susceptibility data show a broad maximum at 5 K, which then decreases at lower temperatures. The $\chi_M T$ value is 4.41 cm^3 M^{-1} K ($\mu_{eff} = 5.94$ B.M.), from room temperature to 120 K, which is close to the expected value for an isolated Mn (II) ion (4.38 cm^3 M^{-1} K with $g = 2$). Below 120 K, the $\chi_M T$ value decreases gradually at first and then sharply: at 1.8 K reaching 0.322 cm^3 M^{-1} K ($\mu_{eff} = 1.61$ B.M.). This behavior indicates the occurrence of weak antiferromagnetic interactions between manganese ions. The magnetic susceptibility data were analyzed in terms of the analytical expression derived by Fisher [21] for an infinite chain of classical spins based on the Hamiltonian $H = -J\sum S_i \cdot S_{i+1}$, for local spin values of $S = 5/2$,

$$\chi = \frac{Ng^2\beta^2 S(S+1)}{3kT}\frac{1+u}{1-u} \tag{1}$$

with $u = \coth\left[\frac{JS(S+1)}{kT}\right] - \left[\frac{kT}{JS(S+1)}\right]$.
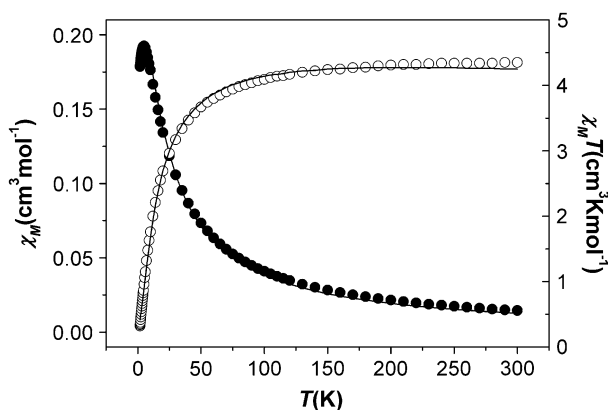

Figure 4. The χ_M (●) and $\chi_M T$ (○) *vs.* *T* plots for **1**. The solid line represents the best least-square fit with the parameters given in the text.
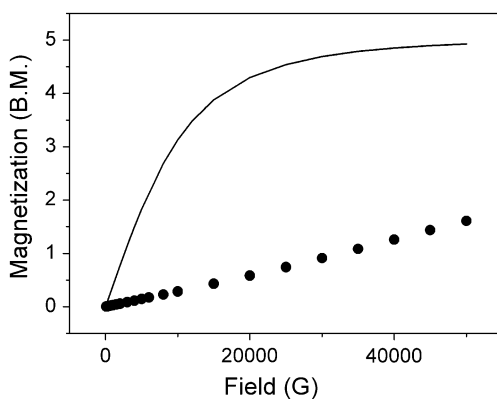
Figure 5. Magnetization *vs*. magnetic field dependence at 2 K. The solid line is the Brillouin function for $S = 5/2$ with $g = 2$.

The best least-squares fit gives the parameters $J = -1.38(3)$ cm^{-1} and $g = 2.00(1)$, with $R = 3 \times 10^{-4}$ (paramagnetic impurity 3%).

Magnetization data at 2 K were collected from 0 to 50 000 G (figure 5). The experimental data lie below the $M/N\beta$ calculated value for an isolated $S = 5/2$ ion, thus confirming the antiferromagnetic coupling in **1**.

3.4. *IR spectroscopic characterization*

The IR spectrum of 5-amino-1-H-tetrazole has previously been interpreted [22]. Strong absorptions for the amino group of 5-ATZ were observed at 3390 and 3311; a peak at 3175 cm^{-1} was assigned to ring NH stretch. The N–H stretching region of **1** (bands at 3400, 3314, 3210, 3080, and 3019 cm^{-1}) shows increased complexity as a result of intra- and intermolecular hydrogen bonding of the NH and NH$_2$ groups. The dominant peak at 1652 cm^{-1} can be attributed to NH$_2$ group (scissoring mode) of 5-ATZ, seen at 1631 cm^{-1} in its spectrum. Bands arising in the heterocyclic ring stretching region, 1600–1400 cm^{-1}, cannot be easily distinguished. However, a smaller intensity band at 1578 cm^{-1} can be assigned to the C=N stretching frequency [22] (1585 cm^{-1} in the 5-ATZ spectrum). The absorption bands at 1200–1000 cm^{-1} are characteristic of skeletal vibrations of the heterocycle.

4. Discussion

Dichloro-bridged chains built up from edge-sharing octahedra represent a common structural motif [8]. If the two donor ligands in the polymer occupy axial *trans* positions in a distorted Mn octahedron, the resulting chains are linear with two metal–chloride bonds being almost equal [1, 9(b), 16(a)–(c)] or of the same length [16(d)]. **1** shares a common feature with the structural studies cited above. The intermetal distance in the chain direction corresponds to the shortest lattice parameter.

In the case of 2,2′-bipyridine [9(d)], 1,10-phenanthroline [9(e)] and N,N,N′,N′-tetramethylethylenediamine [9(f)] bind to *cis* sites in the coordination octahedron around Mn(II) cation. As a result, the bridging chlorides are not arranged in a coplanar fashion and a zig-zag rather than a linear chain is formed. Obviously, this geometry is enforced by chelating ligands. In this case, two Mn–Cl distances in the planar Mn_2Cl_2 core are well differentiated, e.g. 2.481 and 2.662 [9(d)], 2.482 and 2.6499 [9(e)], 2.536 and 2.608 Å [9(f)], and deviation from an ideal octahedral geometry is significantly higher.

Chains from edge-sharing octahedra, with all chlorides bridging two Mn(II) cations and the donor ligands in *trans* or *cis* configuration, show both an antiferromagnetic and ferromagnetic coupling [9, 16(d)]. The majority of the compounds demonstrate a rather small value of the exchange parameter ($|J| \leq 1$ cm^{-1}). The metal–chloride bridges, which are common to these chain compounds, provide the primary pathway for magnetic superexchange. As the Mn–Cl distances remain almost constant throughout this entire series of compounds, none of the variations in the ancillary ligands have a significant impact on the exchange coupling in the inorganic chain.

An empirical link between the solid-state structures of **1** and "parent" inorganic solid $MnCl_2$ can be established using a formalism termed dimensional reduction [23]. In the dimensional reduction concept, many low-dimensional networks can be described as segments of higher dimensional metal halide frameworks [24]. For example, small dialkylammonium cations were used as molecular "scissors" to obtain ribbon structures based on edge-sharing octahedra derived from the parent hexagonal $CdCl_2$ lattice [24(c)]. Infinite layers of edge-sharing $MnCl_6$ octahedra in the hexagonal lattice of manganese chloride [(Mn–Cl 2.552(3) Å, ∠Cl–Mn–Cl 86.72(6)°, 93.28(6)°, Mn···Mn 3.711 Å] [25] can be viewed as built of parallel $(MnCl_2)_n$ chains that are offset with respect to each other by 1.86 Å along the chain such that every Cl from one chain is coordinated to the apical octahedral position of the Mn of the other chain (figure 6). Coordination of 5-ATZ to the manganese cation in **1** "cuts" the Mn–Cl–Mn bridges of the parent lattice and stabilizes 1-D ligand-substituted fragments of the layers.

Isomorphism of **1** and $[Cd(5-ATZ)_2Cl_2]_n$ [12] is worth mentioning. This finding prompted us to look for other dichloro-bridged chain polymers of these metals with the same ligands to check if it is a particular case or a tendency. A Cambridge Structural Database (CSD) search [26] revealed at least six more pairs of isomorphous Mn and Cd polymers of this family (table 3). We are tempted to speculate that dimensional reduction generated by organic ligands toward the isomorphous $MnCl_2$ and $CdCl_2$ [27] parent networks results in Mn(II) and Cd(II) polymeric hybrid structures of the same ligand that are also isomorphous. The isostructural nature of **1** and its cadmium analog implies that it should be possible to prepare solid solutions of these compounds.
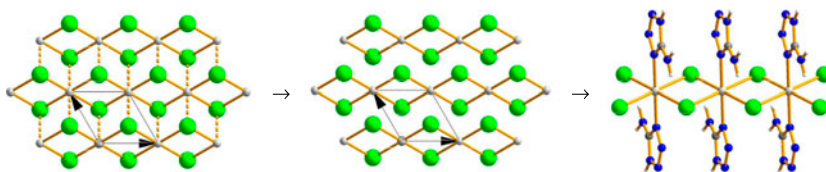

Figure 6. Deconstruction of the $MnCl_2$ framework of edge-sharing octahedra. Addition of 5-ATZ ligand "cuts" the Mn–Cl–Mn bridges to give 1-D ligand-substituted chains.

Table 3. The lattice parameters of Cd(II) and Mn(II) dichloro-bridged chain polymers and inorganic MCl_2 solids.

Compound and CSD refcode	Unit cell parameters					
	a (Å)	b (Å)	c (Å)	α (°)	β (°)	γ (°)
$CdCl_2$ [27]	3.8459(1)	3.8459(1)	17.4931(4)	90.00	90.00	120.00
$MnCl_2$ [25]	3.711(2)	3.711(2)	17.59(7)	90.00	90.00	120.00H
$[M(\mu_2\text{-}Cl)_2L]_n$						
L = 1,10-phenanthroline						
M = Cd, OLOJUU	16.860(1)	10.521(0)	7.232(0)	90.00	110.30(0)	90.00
M = Mn, HAVDAK	17.245(1)	10.443(0)	7.035(0)	90.00	111.98(0)	90.00
L = 2,2′-bipyridine						
M = Cd, EKEVAR	17.552(0)	9.317(0)	7.171(0)	90.00	110.86(0)	90.00
M = Mn, YOLHAI	7.007(1)	9.200(1)	16.495(1)	90.00	91.31(0)	90.00
L = N,N,N′, N′-tetramethylethylenediamine						
M = Cd, ZZZAJG	7.260(20)	10.760(20)	14.470(20)	90.00	91.50(20)	90.00
M = Mn, TOTHAL	7.062(1)	10.656(2)	14.432(3)	90.00	91.63(2)	90.00
$[M(\mu_2\text{-}Cl)_2L_2]_n$						
L = benzotriazole						
M = Cd, CIFVES	23.125(4)	3.818(2)	16.680(4)	90.00	100.61(2)	90.00
M = Mn, CIFVIW	23.441(5)	3.728(1)	16.480(3)	90.00	98.50(2)	90.00
L = benzoselenadiazole						
M = Cd, ZIJRIV	3.777(1)	9.284(4)	10.824(5)	78.81(0)	82.42(0)	82.51(0)
M = Mn, ZIJROB	3.720(1)	9.278(2)	10.769(3)	80.06(0)	81.25(0)	83.35(0)
L = pyrazole						
M = Cd, LEDQIV	18.311(0)	3.863(0)	13.957(0)	90.00	95.57(1)	90.00
M = Mn, DCPZMN	18.260(20)	3.761(2)	13.839(2)	90.00	94.78(8)	90.00

5. Conclusion

A new Mn(II) dichloro-bridged chain polymer was synthesized from the reaction of 5-ATZ and $MnCl_2 \cdot 4H_2O$ and isolated by the solution evaporation method at room temperature. **1** is structurally close to other manganese polymers of this type. Obviously, conventional conditions of synthesis did not encourage 5-ATZ to demonstrate its capability to bridge metal atoms in various coordination modes with the nitrogens of the tetrazole ring; special efforts (temperature, high pressure, structure directing agents) are required to prepare coordination networks of higher dimensionality. **1** can potentially be applied as an insulating magnetic material, as a dopant in dielectric and conducting polymer composite films to make multifunctional materials. Successful introduction of 5-(2-pyridyl)tetrazole and the secondary metal manganese into the molybdenum oxide complex [28] indicates the possibility of employing **1** as a precursor in the preparation of new metal oxide-based organic–inorganic hybrid materials.

Supplementary material

CCDC 1006111 contains the supplementary crystallographic data for this paper. These data can be obtained free of charge from the Cambridge Crystallographic Data Center via www.ccdc.cam.ac.uk/data_request/cif.

Acknowledgement

Funding

References

[1] A.K. Cheetham, C.N.R. Rao, R.K. Feller. *Chem. Commun.*, **42**, 4780 (2006).
[2] A.K. Cheetham, P.M. Forster. In *Chemistry of Nanomaterials*, C.N.R. Rao, A. Müller, A.K. Cheetham (Eds), pp. 589–619, Wiley-VCH, Weiheim (2003).
[3] (a) N. Roques, V. Mugnaini, J. Veciana. In *Functional Metal-organic Frameworks: Gas Storage, Separation and Catalysis*, M. Schröder (Ed.), pp. 207–258, Springer-Verlag, Berlin (2010); (b) F.A.A. Paz, J. Klinowski, S.M.F. Vilela, J.P.C. Tomé, J.A.S. Cavaleiro, J. Rocha. *Chem. Soc. Rev.*, **41**, 1088 (2012).
[4] A.K. Cheetham, C.N.R. Rao. *Science*, **318**, 58 (2007).
[5] (a) J.S. Miller, M. Drillon. *Magnetism: Molecules to Materials. Models and Experiments*, Vol 1; *Molecule-based Magnets*, Vol 2; *Nanosized Magnetic Materials*, Vol 3, Wiley-VCH, Weinheim (2001); (b) L. Öhrström, K. Larsson. *Molecule-Based Materials: The Structural Network Approach*, B.V. Elsevier, Amsterdam (2005).
[6] N.A. Spaldin. *Magnetic Materials: Fundamentals and Applications*, p. 273, Cambridge University Press, Cambridge (2010).
[7] B.G. Park, J. Wunderlich, X. Martí, V. Holý, Y. Kurosaki, M. Yamada, H. Yamamoto, A. Nishide, J. Hayakawa, H. Takahashi, A.B. Shick, T. Jungwirth. *Nat. Mater.*, **10**, 347 (2011).
[8] U. Englert. *Coord. Chem. Rev.*, **254**, 537 (2010).
[9] See for example: (a) P.M. Richards, R.K. Quinn, B. Morosin. *J. Chem. Phys.*, **59**, 4474 (1973); (b) W. Zhang, J.R. Jeitler, M.M. Turnbull, C.P. Landee, M. Wei, R.D. Willett. *Inorg. Chim. Acta*, **256**, 183 (1997); (c) J.-Z. Wu, S. Tanase, E. Bouwman, J. Reedijk, A.M. Mills, A.L. Spek. *Inorg. Chim. Acta*, **351**, 278 (2003); (d) I. Romero, M. Rodríguez, A. Llobet, M. Corbella, G. Fernández, M.-N. Collomb. *Inorg. Chim. Acta*, **358**, 4459 (2005); (e) A. Majumder, M. Westerhausen, A.N. Kneifel, J.-P. Sutter, N. Daro, S. Mitra. *Inorg. Chim. Acta*, **359**, 3841 (2006); (f) P. Sobota, J. Utko, S. Szafert, Z. Janas, T. Glowiak. *J. Chem. Soc., Dalton Trans.*, 3469 (1996); (g) J.D. Martin, R.F. Hess, P.D. Boyle. *Inorg. Chem.*, **43**, 3242 (2004).
[10] (a) R. Dingle, M.E. Lines, S.L. Holt. *Phys. Rev.*, **187**, 643 (1969); (b) R.E. Caputo, R.D. Willett. *Phys. Rev. B*, **13**, 3956 (1976); (c) K. Takeda, J.C. Schouten, K. Kopinga, W.J.M. de Jonge. *Phys. Rev. B*, **17**, 1285 (1978).
[11] F.-H. Zhao, Y.-X. Che, J.-M. Zheng. *Inorg. Chem.*, **51**, 4862 (2012).
[12] Y.-L. Yao, L. Xue, Y.-X. Che, J.-M. Zheng. *Cryst. Growth Des.*, **9**, 606 (2009).
[13] (a) X.-W. Wang, J.-Z. Chen, J.-H. Liu. *Cryst. Growth Des.*, **7**, 1227 (2007); (b) X. Xue, B.F. Abrahams, R.-G. Xiong, X.-Z. You. *Aust. J. Chem.*, **55**, 495 (2002); (c) T.-W. Wang, D.-S. Liu, C.-C. Huang, Y. Sui, X.-H. Huang, J.-Z. Chen, X.-Z. You. *Cryst. Growth Des.*, **10**, 3429 (2010); (d) T. Panda, P. Pachfule, Y. Chen, J. Jiang, R. Banerjee. *Chem. Commun.*, **47**, 2011 (2011).
[14] (a) C. O'Connor. *J. Prog. Inorg. Chem.*, **29**, 203 (1982); (b) G.A. Bain, J.F. Berry. *J. Chem. Educ.*, **85**, 532 (2008).
[15] G.M. Sheldrick. *Acta Cryst.*, **A64**, 112 (2008).
[16] (a) S. Gorter, A.D. Vaningen, G.C. Verschoo. *Acta Crystallogr. B*, **30**, 1867 (1974); (b) I. Sotofte, K. Nielsen. *Acta Chem. Scand. A*, **38**, 257 (1984); (c) L.M. Lee, P.J.W. Elder, P.A. Dube, J.E. Greedan, H.A. Jenkins, J.F. Britten, I. Vargas-Baca. *CrystEngComm*, **15**, 7434 (2013); (d) K.I. Pokhodnya, M. Bonner, A.G. DiPasquale, A.L. Rheingold, J.-H. Her, P.W. Stephens, J.-W. Park, B.S. Kennon, A.M. Arif, J.S. Miller. *Inorg. Chem.*, **46**, 2471 (2007).
[17] K. Britts, I.L. Karle. *Acta Cryst.*, **22**, 308 (1967).
[18] A.P. Golombek, M.P. Hendrich. *J. Magn. Reson.*, **165**, 33 (2003).
[19] S. Blanchard, G. Blain, E. Rivière, M. Nierlich, G. Blondin. *Chem. Eur. J.*, **9**, 4260 (2003).
[20] J.A. Weil, J.R. Bolton, J.E. Wertz. *Electron Paramagnetic Resonance: Elementary Theory and Applications*, Wiley-Interscience, New York (1994).

[21] (a) M.E. Fisher. *Am. J. Phys.*, **32**, 343 (1964); (b) O. Kahn. *Molecular Magnetism*, Wiley-VCH, New York (1993).
[22] H.B. Jonassen, T. Paukert, R.A. Henry. *Appl. Spectrosc.*, **21**, 89 (1967).
[23] E.G. Tulsky, J.R. Long. *Chem. Mater.*, **13**, 1149 (2001).
[24] See for example: (a) J.R. Long, A.S. Williamson, R.H. Holm. *Angew. Chem. Int. Ed.*, **34**, 226 (1995); (b) S. Haddad, F. Awwadi, R.D. Willett. *Cryst. Growth Des.*, **3**, 501 (2003); (c) A. Thorn, R.D. Willett, B. Twamley. *Cryst. Growth Des.*, **6**, 1134 (2006).
[25] J.D. Tornero, J. Fayos. *Z. Kristallogr.*, **192**, 147 (1990).
[26] CSD (version 5.35 February 2014):)F.H. Allen. *Acta Crystallogr., Sect. B: Struct. Sci.*, **B58**, 380 (2002).
[27] D.E. Partin, M. O'Keeffe. *J. Solid State Chem.*, **95**, 176 (1991).
[28] P. Dong, Q.-K. Zhang, F. Wang, S.-C. Chen, X.-Y. Wu, Z.-G. Zhao, C.-Z. Lu. *Cryst. Growth Des.*, **10**, 3218 (2010).